Electronic Supplementary Information

Ultrasmall $FeNi_3N$ particles with exposed active (110) surface anchored on nitrogen-doped graphene for multifunctional electrocatalysts

Lina Liu,[a,b,c] *Feng Yan,*[b] *Kaiyue Li,*[b] *Chunling Zhu,**[a] *Ying Xie,**[d] *Xitian Zhang,*[c] *Yujin Chen**[ab]

[a]*Key Laboratory of Superlight Materials and Surface Technology, Ministry of Education, College of Materials Science and Chemical Engineering, Harbin Engineering University, Harbin 150001, China*

[b]*College of Science, Harbin Engineering University, Harbin 150001, China.*

[c]*Key Laboratory for Photonic and Electronic Bandgap Materials, Ministry of Education, School of Physics and Electronic Engineering, Harbin Normal University, Harbin 150025, China*

[d]*Key Laboratory of Functional Inorganic Material Chemistry, Ministry of Education, School of Chemistry and Materials Science, Heilongjiang University, Harbin 150080, China*

*Corresponding authors
E-mail addresses: zhuchunling@hrbeu.edu.cn (C. Zhu), xieying@hlju.edu.cn (Y. Xie) or chenyujin@hrbeu.edu.cn (Y. Chen).

Experimental details

Chemicals. Graphenes with a later size of 0.5 to 5 μm and thickness of about 0.8 nm, were purchased from Nanjing XFNANO Material Tech Co., Ltd. (Nanjing City, China). Ferric acetylacetonate, nickel acetate, ammonia and potassium hydroxide and were purchased from Sinopharm Chemical Reagent Co., Ltd. (Shanghai City, China). Ethanol was purchased from Tian Fuyu Fine Chemical Co., Ltd. (China). PVA-1788 powder was purchased from Aladdin Industrial Corporation. It is worth noting that, all of the chemicals were purchased without further treatment before using, and all aqueous solutions were prepared using ultrapure water.

Synthesis of the $FeNi_3N$/NG. The synthesis of $FeNi_3N$/NG composite involved a simple two-step process. At first, 36 mg of graphene was dispersed in 72 ml ethanol, then 57 mg of ferric acetylacetonate and 150 mg of nickel acetate was added to the mixture above, sequentially. Distilled water (3.6 ml) and ammonia (2 ml) was added to the mixture with sonication 15 min. The resultant mixture was sealed in a conical flask with lid, and kept at 80^oC for 10 h under stirring. The precipitates were washed with distilled water and ethanol for several times, then centrifuged and dried in a vacuum oven at 40 ^oC. In this step, the NiFe hydroxide/G was obtained. The NiFe hydroxide/G was annealed under NH_3 atmosphere at 500 ^oC for 2 h with a ramp rate of 5 ^oC/min. After cooling to room temperature, the $FeNi_3N$/NG was obtained.

Synthesis of the Ni-N/NG. The Ni-N/NG was prepared through the same process as that of $FeNi_3N$/NG except that Fe source was not added to the reaction system and the amount of nickel acetate was changed to 190 mg.

Synthesis of the Fe_2N/NG. The Fe_2N/NG was prepared through the same process as that of $FeNi_3N$/NG except that Ni source was not added to the reaction system and the amount of ferric acetylacetonate was changed to 270.5 mg.

Synthesis of the $FeNi_3N$/NG with different atomic ratio of Ni to Fe. $FeNi_3N$/NG-1 and $FeNi_3N$/NG-2 were prepared through the same process as that of $FeNi_3N$/NG except that the amounts of ferric acetylacetonate and nickel acetate were different. The amounts of ferric acetylacetonate and nickel acetate were 45 and 158.5 mg for the former, respectively, while were changed to 77.1 and 135.8 mg, respectively, for the latter.

Characterizations. The morphology and size of as prepared catalyst were characterized by an FEI Tecnai-F20 transmission electron microscope equipped with a Gatan imaging filter (GIF); and the energy-dispersive X-ray analysis (EDX) and elemental mapping were also performedusing Tecnai-F20 instrument. To further confirm the structures of our catalyst, XRD was performed on a Rigaku D/max-2600/PC with Cu Kα radiation (λ=1.5418Å), and XPS analyses were carried out on a Thermo ESCALAB250 X-ray Photoelectron Spectrometer.

Electrochemical measurement. The electrochemical activities of our catalysts toward overall oxygen reactions (ORR and OER) were performed in a three-electrode system (CHI 760D, CH Instrument, USA), and graphite rod was used as a counter electrode and Ag/AgCl (KCl saturated) was employed as a reference electrode. Preparation of working electrode was as follows: Firstly, 5 mg of the $FeNi_3N$/NG catalyst powder was dispersed in 450 μL ethanol, and 50 μL of 5.0 wt% Nafion solution was added. Then above mixture was sonicated for at least two hours to form a relatively homogeneous catalyst ink. 10.0 μL of the catalyst ink (0.1 mg) was droped onto the surface of a polished glassy carbon rotating disk electrode with a disk diameter of 5.0 mm, and then used as working electrode for electrochemical measurements after the solvent was evaporated completely in air. The LSV curves of ORR were performed at a rotating rate ranging from 400 to 2025 rpm on RDE electrode in 0.1 M saturated KOH solution with a scan rate of 5 mV s^{-1}. Furthermore, the CV measurements toward ORR were taken at a scan rate of 50 mV s^{-1} in 0.1 M O_2-saturated and Ar_2-saturated KOH solution. And the OER activity were evaluated using LSV measurement in 0.1 M KOH solution at a scan rate of 5 mV s^{-1}. All potentials measured in this study were calibrated to reversible hydrogen electrode (RHE) according the following Equation: $E_{(RHE)} = E_{(Ag/AgCl)} + 0.21 \text{ V} + 0.059 \times \text{pH}$.

Electrochemical measurements of the catalysts toward HER and OER were performed using a standard three-electrode system in 1 M KOH solution by an electrochemical station (CHI660E, CH Instrument, USA). The carbon paper coated by catalyst slurry were used as working electrode, while graphite rod and a Ag/AgCl (KCl saturated) as counter and reference electrodes, respectively. The mass loading and coating area of the catalysts was approximately 2 mg cm^{-2} and 1 cm^{-2} for the working electrodes, respectively. The HER and OER activity were evaluated using Linear sweep voltammetry (LSV) measurement in 1 M KOH solution with a scan rate of 5 mV s^{-1} at room temperature. Furthermore, the Tafel slopes were obtained according the corresponding LSV curves and calculated from the following Tafel equation: $\eta = a + b \log |j|$, where η represents the overpotential, j represents cathodic current density, a is the Tafel constant, and b is the Tafel slope.

Liquid Zn-air battery assembly. For the liquid Zn-air battery test of our catalyst, the certain volume of pre-prepared catalyst ink (same as that for ORR electrodes) was coated uniformly onto a carbon paper with a catalyst loading of 0.5 mg cm^{-2} as air electrode. A polished zinc plate with thickness of 0.25 mm was used as the anode, and electrolyte for primary Zn-air batteries was 6M KOH, while that was 6 M KOH containing 0.2 M $Zn(CH_3COO)_2$ for rechargeable Zn-air batteries. Measurements of the home-made liquid Zn-air battery were carried out using an electrochemical work-station (CHI 660E, CH Instrument, USA) at 25 ^oC; and the specific capacity and power density were obtained from the Galvanostatical discharge results.

Solid-state Zn-air battery assembly. For the assembled all-solid-state Zn-air battery, a polished zinc plate with thickness of 0.25 mm was used as anode, and a certain volume of catalyst ink was droped onto a cleaned carbon fiber cloth substrate (1.5 × 3 cm^2) with a catalyst loading of 1.50 mg cm^{-2} as the air electrode. The preparation process of the gel polymer electrolyte was as follows: firstly, polyvinyl alcohol (PVA-

1788, 5 g) powder was dissolved in 50.0 mL deionized water at 90 °C under stirring for 2.0 h. Then 5.0 mL of 18.0 M KOH containing 0.02 M $Zn(CH_3COO)_2$ was added into above mixture, and the electrolyte solution kept stirring at 90 °C, until the solution became uniform about 30 min. Secondly, the above solution was poured into a square glass groove to form a thin film, after freezed using afreezer at -10 °C over 12 h, then thawed at room temperature. Then the all-solid-state Zn-air battery was assembled by place the as-prepared air electrode and zinc plate on the two sides of PVA gel (1.5 cm×2 cm×0.5 cm), then a piece of pressed Ni foam was used as current collector next to the air electrolyte. Finally, a polymer film and tapes was used to assemble the solid-state Zn-air battery.

DFT Computational Methods. Density functional theory (DFT) calculations were performed by using the CASTEP packages.[1] The exchange-correlation energies were calculated according to the Perdew-Wangscheme within the general gradient approximation (GGA) framework.[2,3] With the application of the ultrasoft potential (Vanderbilt, D. Phys. ReV. B 1990, 41, 7892), the energy cutoff was 340 eV. The integration of Brillouin-zone was treated by a (6×4×1) grid, and a vacuum region (15 Å) was added above each slab to aviod the fake interaction along z axis. Stable configurations were obtained by a geometry optimization, and the iteractions were repeated until the forces on the atoms were less than 0.1 eV/Å and the energy change less than 1.0×10^{-5}eV. The adsorption energy (E_{ads}) is defined as the following equation:

$$E_{ads} = E_{surf + O_2} - E_{surf} - E_{O_2} \tag{1}$$

where $E_{surf + O_2}$, E_{surf}, and E_{O_2} are the total energies of the O_2/material systems, the material surface, and the free O_2 molecule, respectively. In this definition, a negative value of E_{ads} signifies a high stability of adsorption O_2.

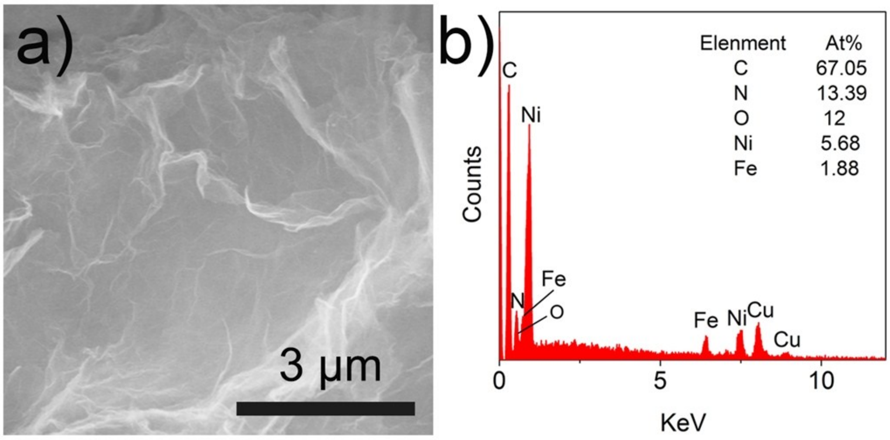

Fig. S1. (a) SEM images of $FeNi_3N$/NG, and (b) Energy-dispersive X-ray (EDX) spectrum and corresponding elemental contents of the $FeNi_3N$/NG (The signal of Cu arises from the SEM substrate made of copper).

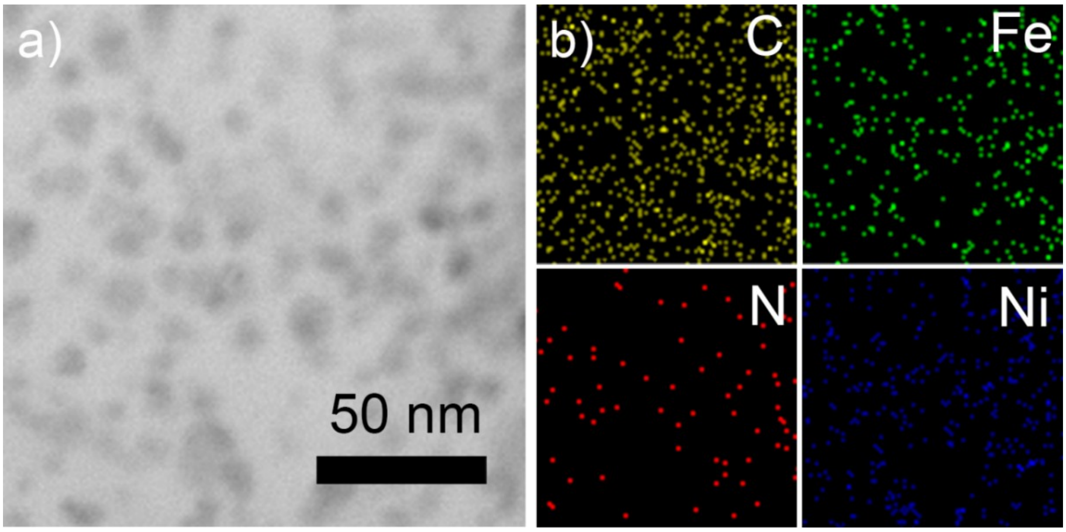

Fig. S2. (a) STEM) image and (b) EDX elemental mappings of $FeNi_3N$/NG.

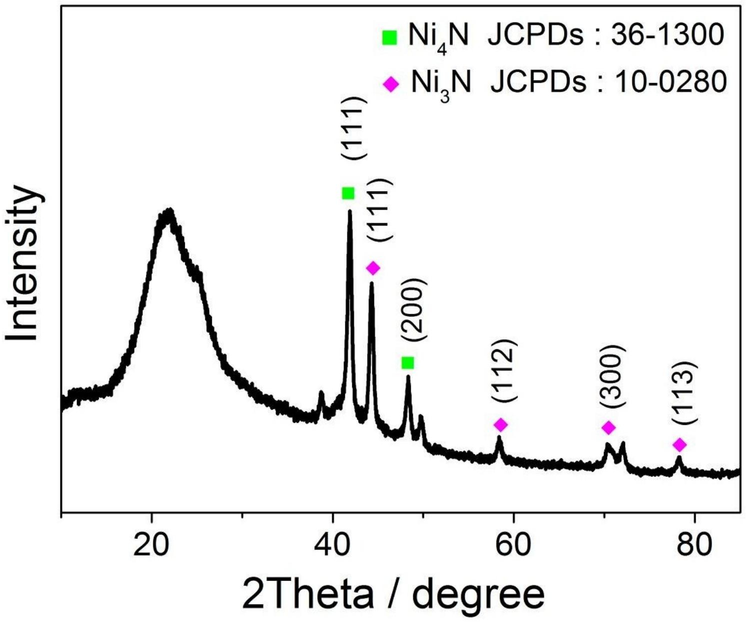

Fig. S3. The XRD patterns of Ni-N/NG

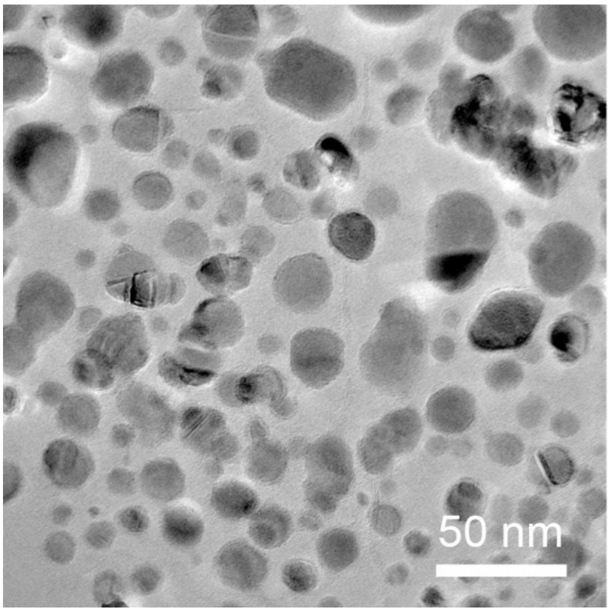

Fig. S4. TEM image of the Ni-N/NG.

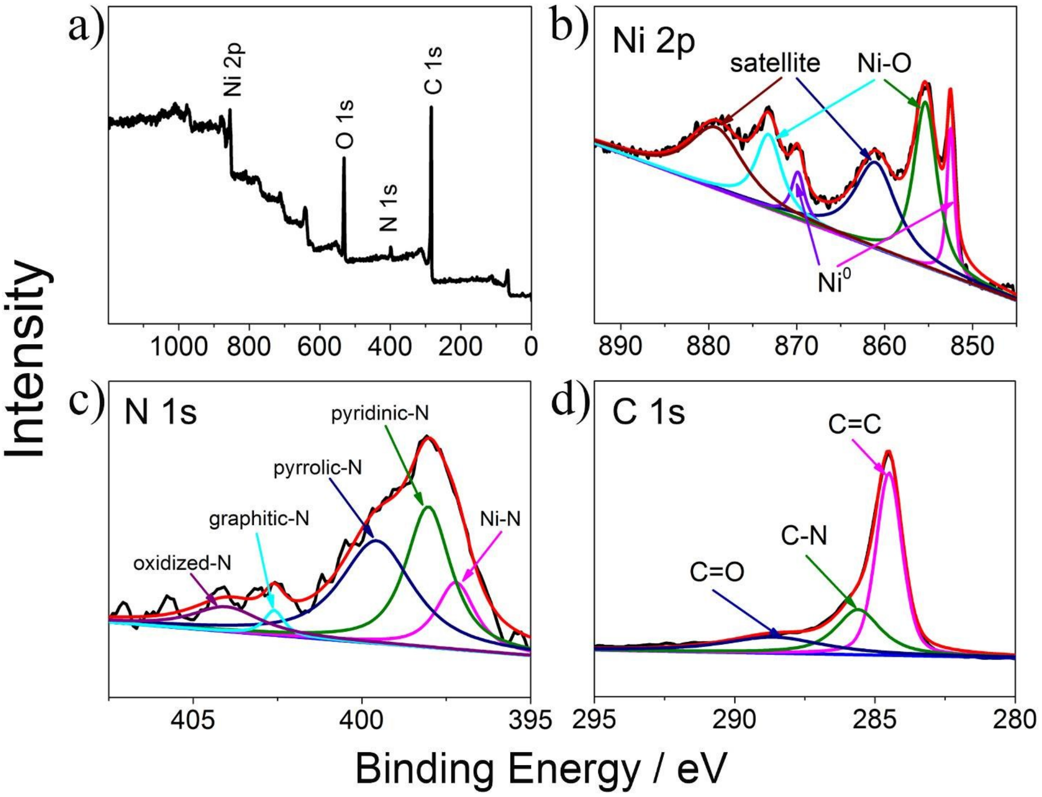

Fig. S5. XPS spectra of the Ni-N/NG. The XPS survey spectrum (a), Ni 2p (b), N1s (c) and C 1s (d).

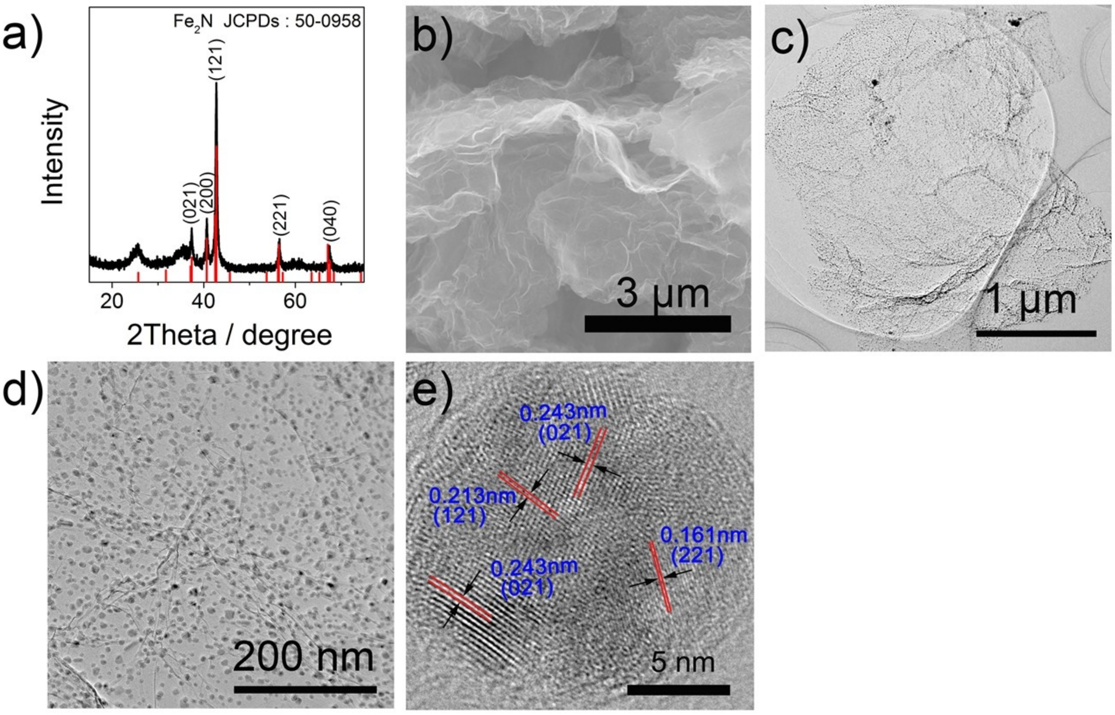

Fig. S6. (a) XRD patterns, (b) SEM image of Fe_2N/NG. (c-e) TEM images of the Fe_2N/NG with different magnifications.

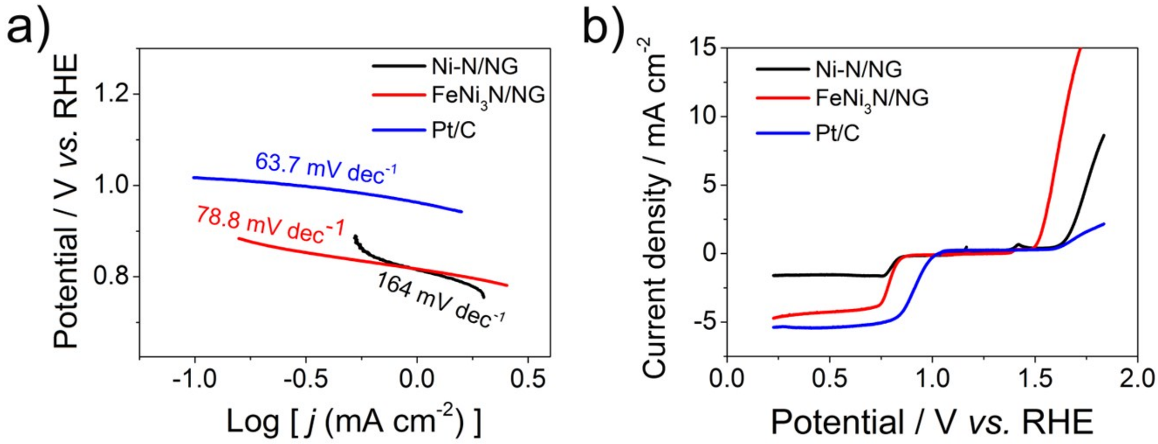

Fig. S7. (a) The Tafel slopes of $FeNi_3N$/NG, Ni-N/NG and Pt/C toward ORR. (b) The LSV curves of $FeNi_3N$/NG, Ni-N/NG and Pt/C for both ORR and OER in 0.1 M KOH at a rotation speeds of 1600 rpm and a sweep rate of 5 mV s^{-1}.

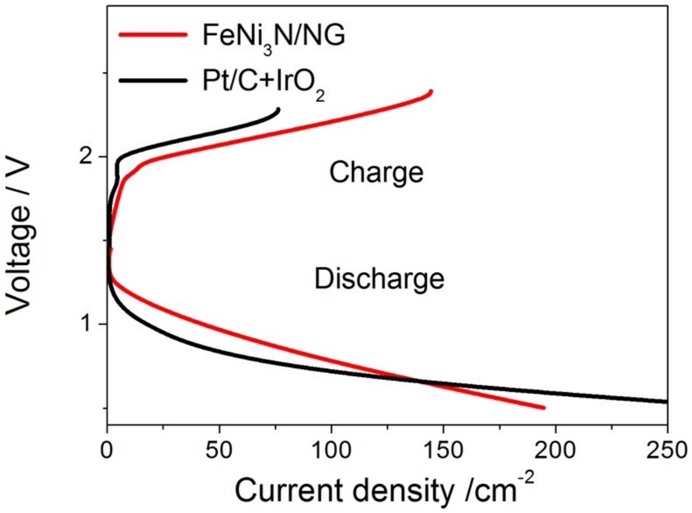

Fig. S8. The charging and discharging polarization curves of rechargeable Zn-air batteries based on the $FeNi_3N$/NG and Pt/C+ IrO_2 cathodes.

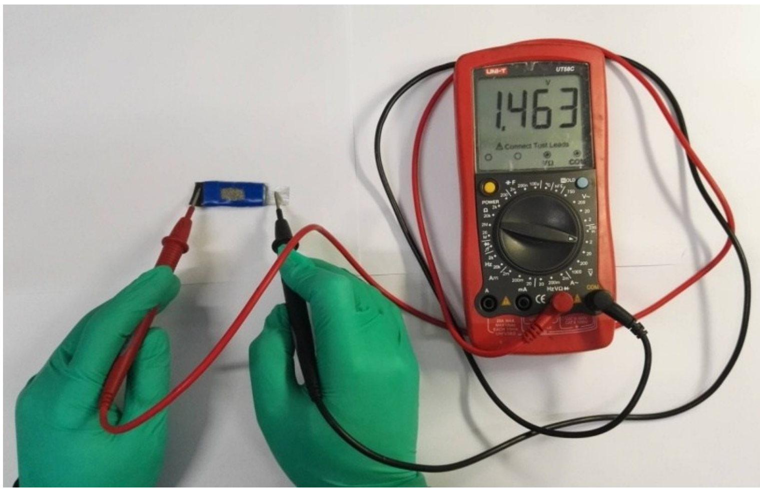

Fig. S9. The open-circuit voltage of one all-solid-state Zn-air battery.

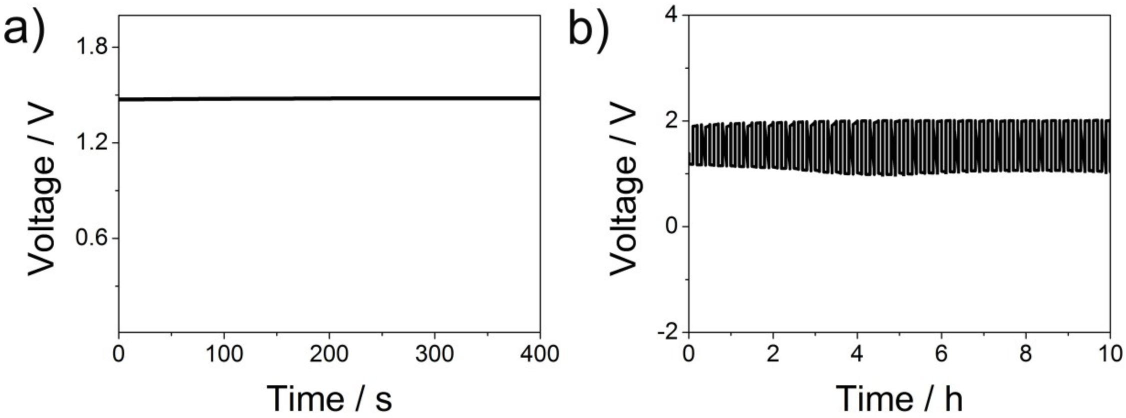

Fig. S10. (a) Open-circuit plots of one all-solid-state Zn-air battery. (b) Galvanostatic charge-discharge cycling curves of rechargeable all-solid-state Zn-air battery at 10 mA cm^{-2}.

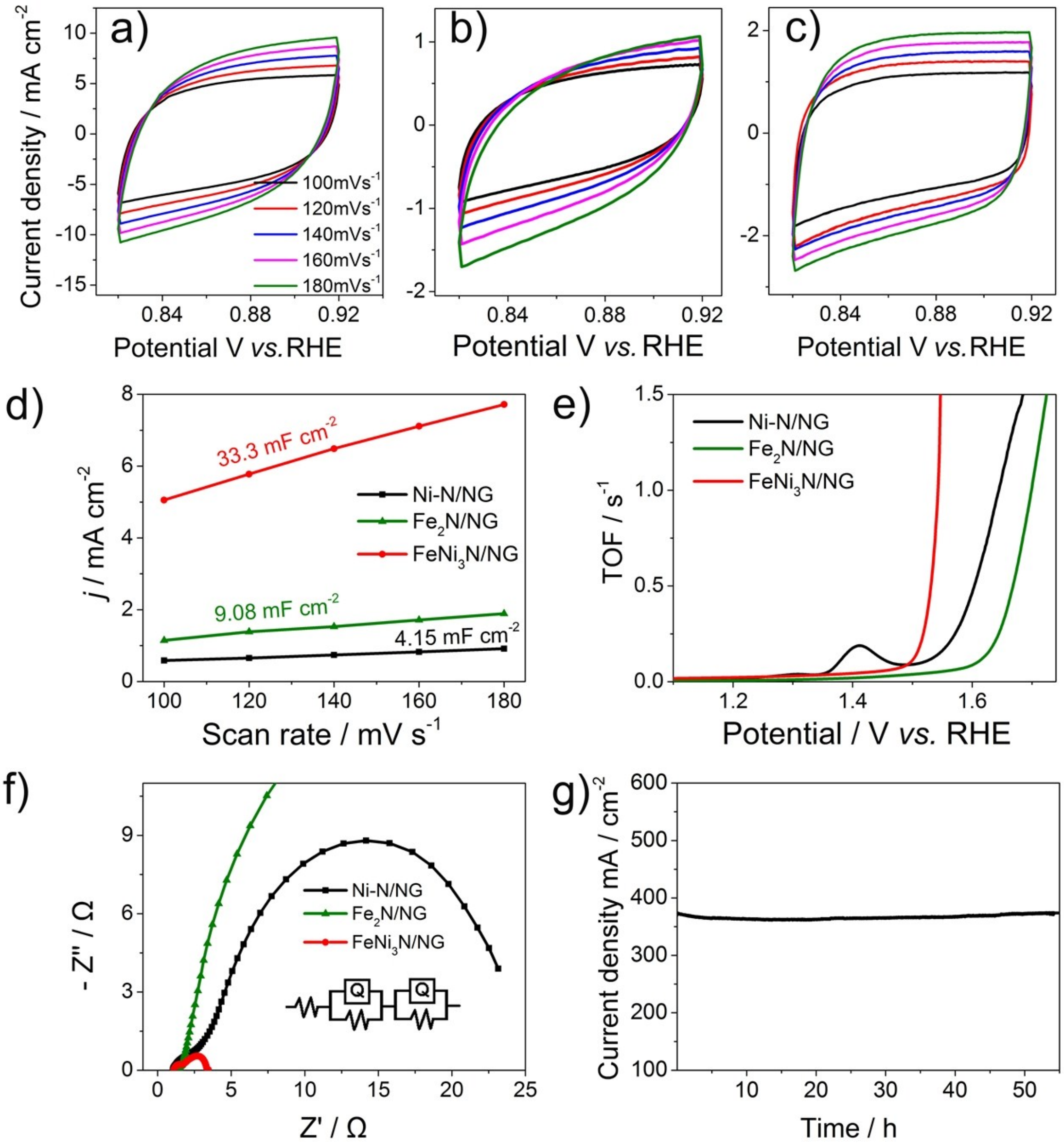

Fig. S11. (a,b,c) The cyclic voltammograms curves of $FeNi_3N/NG$, Ni-N/NG and Fe_2N/NG in the region of 0.836- 0.936 V *vs*. RHE in 1.0 M KOH for OER. (d) The electrochemical double-layer capacitances of $FeNi_3N/NG$, Ni-N/NG and Fe_2N/NG toward OER. (e) The calculated TOF data of $FeNi_3N/NG$, Ni-N/NG and Fe_2N/NG for OER. (f) The Nyquist plots of $FeNi_3N/NG$, Ni-N/NG and Fe_2N/NG for OER at η = 290 m V, and the inset shows the corresponding equivalent circuit. (g) Long-term stability of $FeNi_3N/NG$ for OER at a given overpotential of 340 mV.

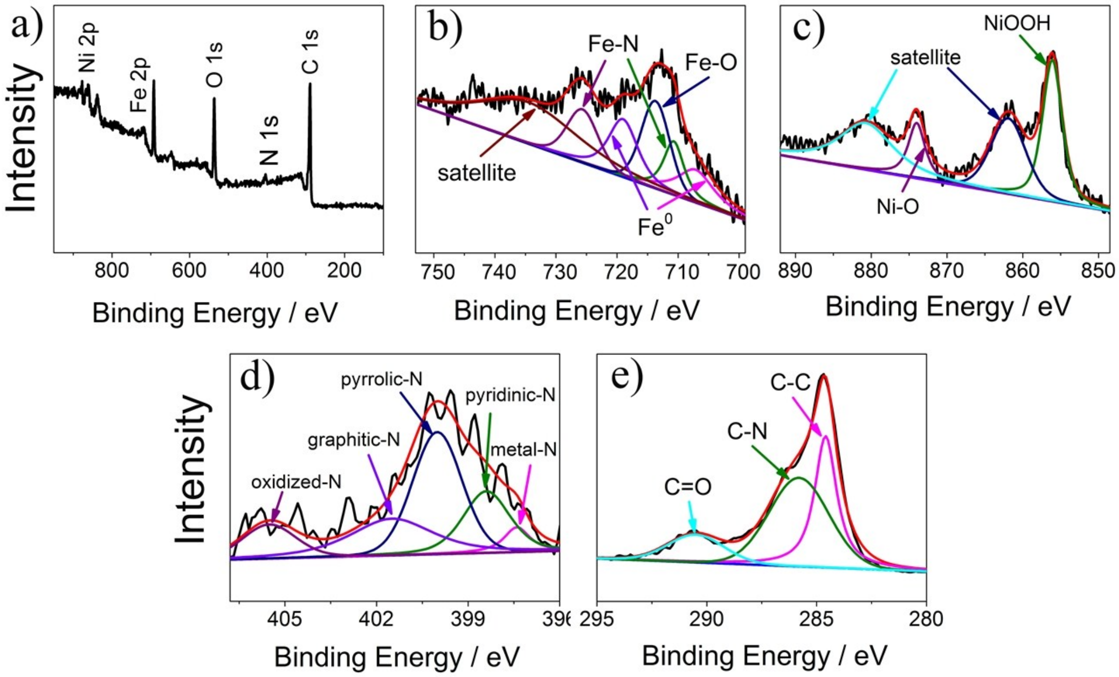

Fig. S12. XPS spectra of the $FeNi_3N$/NG after OER. The XPS survey spectrum (a), Fe 2p (b), Ni 2p (c), N1s (d) and C 1s (e).

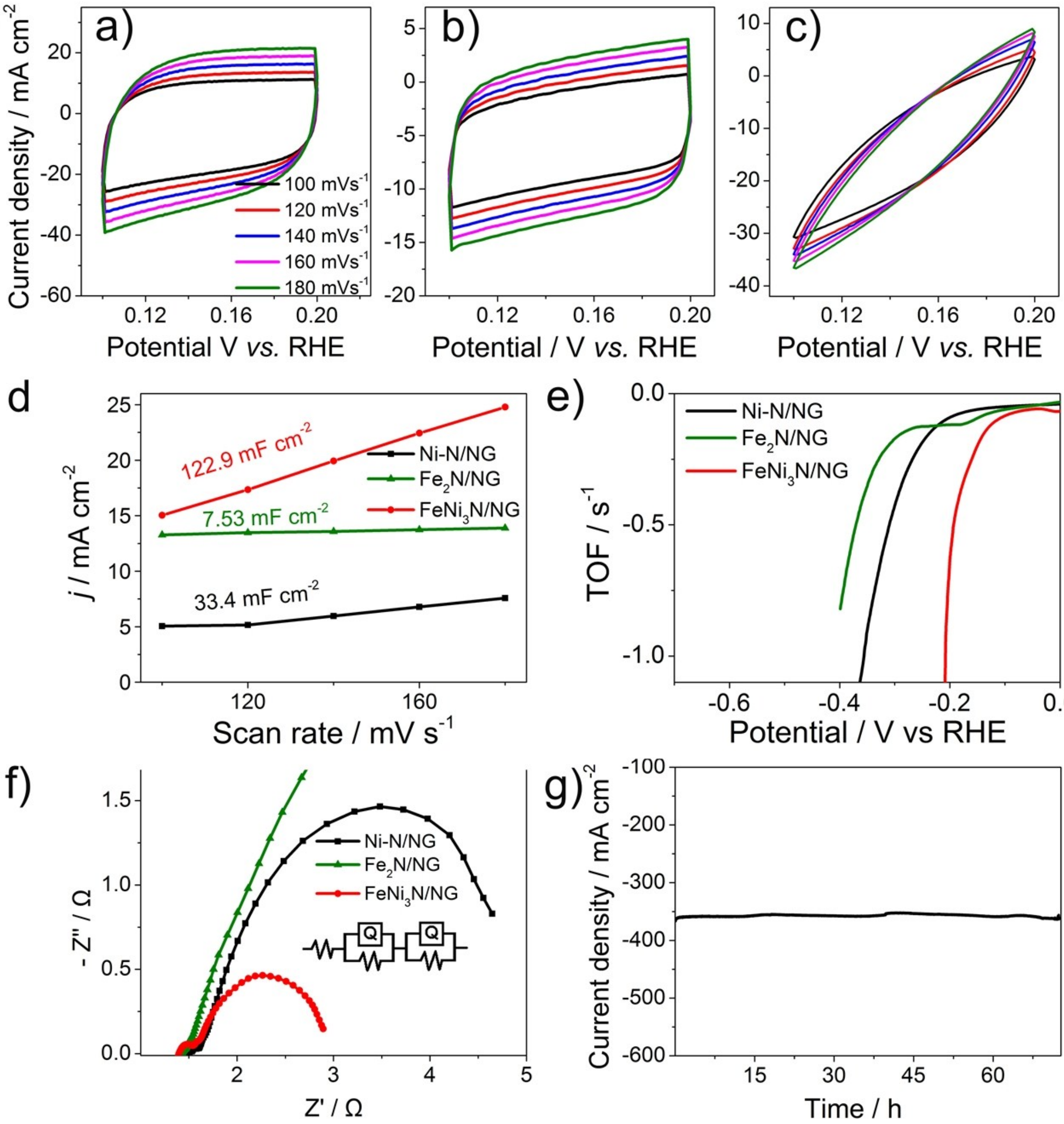

Fig. S13. (a,b,c) Thecyclic voltammograms curves of FeNi$_3$N/NG, Ni-N/NG and Fe$_2$N/NG in the region of 0.1-0.2 V *vs*. RHE in 1.0 M KOH for HER. (d) The electrochemical double-layer capacitances of FeNi$_3$N/NG, Ni-N/NG and Fe$_2$N/NG toward HER. (e) The calculated TOF data of the FeNi$_3$N/NG, Ni-N/NG and Fe$_2$N/NG for HER. (f) The Nyquist plots of FeNi$_3$N/NG, Ni-N/NG and Fe$_2$N/NG for HER at η = 300 m V, and the inset shows the corresponding equivalent circuit. (g) Long-term stability of FeNi$_3$N/NG for HER at a given overpotential of 255 mV.

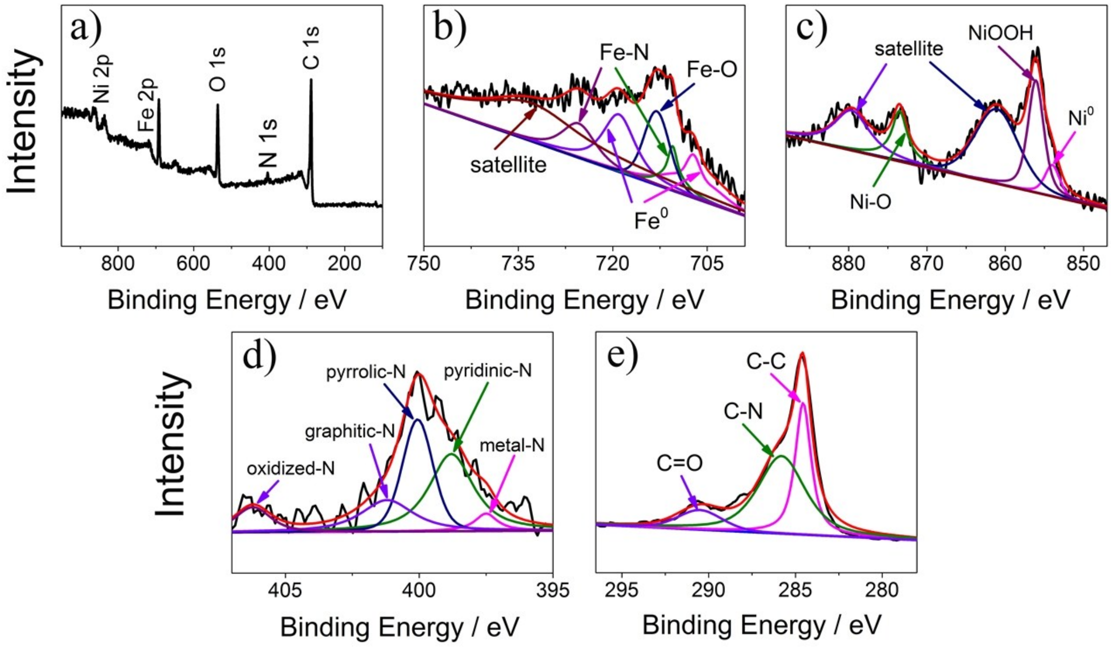

Fig. S14. XPS spectra of the $FeNi_3N$/NG after HER. The XPS survey spectrum (a), Fe 2p (b), Ni 2p (c), N1s (d) and C 1s (e).

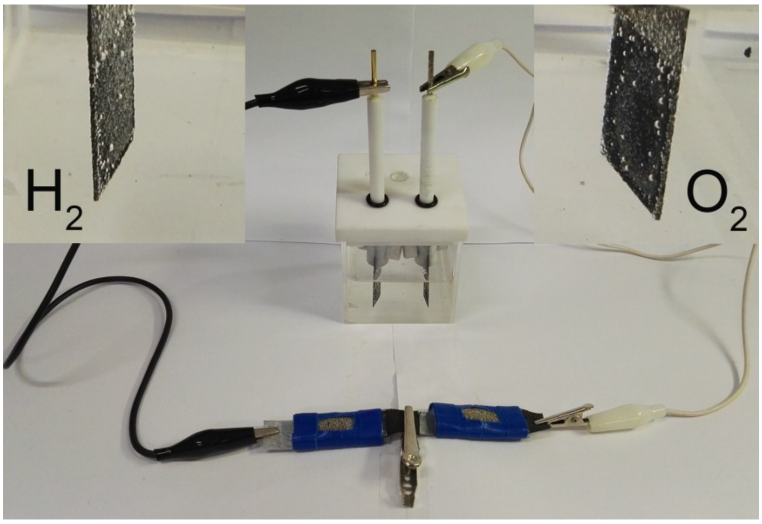

Fig. S15. The photograph of the two-electrode electrolyser based on the $FeNi_3N$/NG powered by two all-solid-state Zn-air batteries with the $FeNi_3N$/NG air cathode in series.

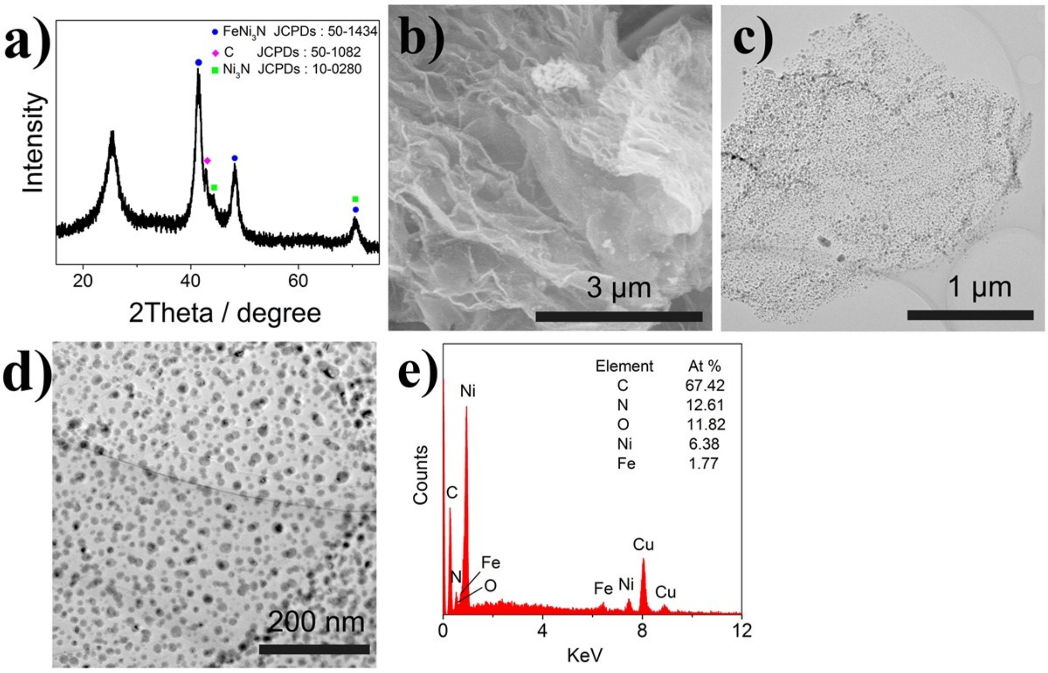

Fig. S16. (a) The XRD pattern, (b) low -magnification SEM image, (c,d) TEM images with different magnifications, and (e) EDX spectrum and corresponding elemental contents of FeNi$_3$N/NG-1. (The signal of Cu arises from the SEM substrate made of copper).

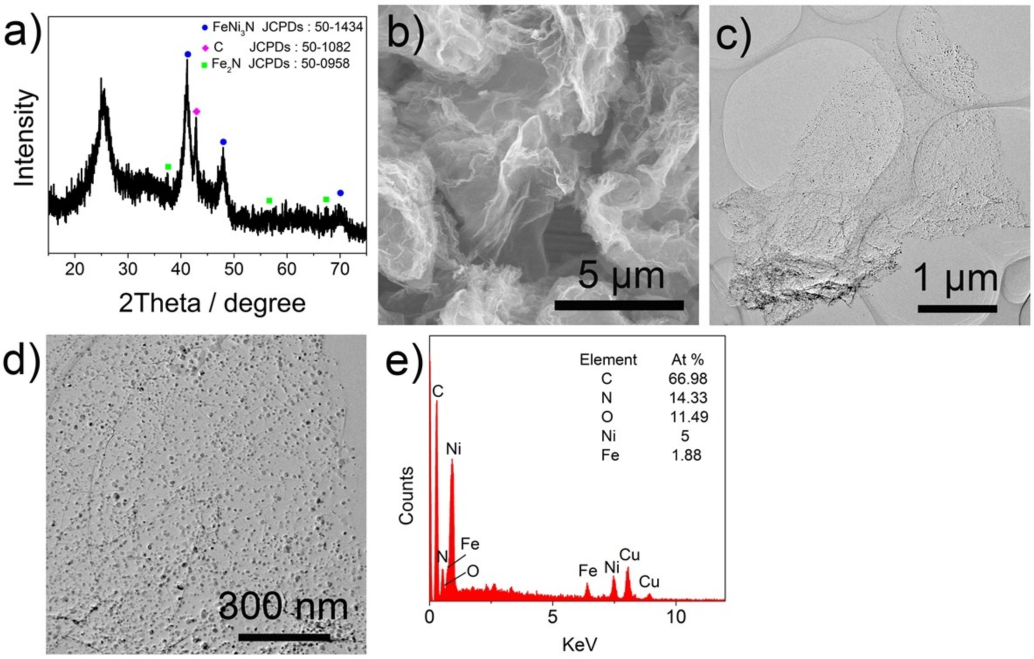

Fig. S17. (a) The XRD pattern, (b) low -magnification SEM image, (c,d) TEM images with different magnifications, and (e) EDX spectrum and corresponding elemental contents of of FeNi$_3$N/NG-2. (The signal of Cu arises from the SEM substrate made of copper).

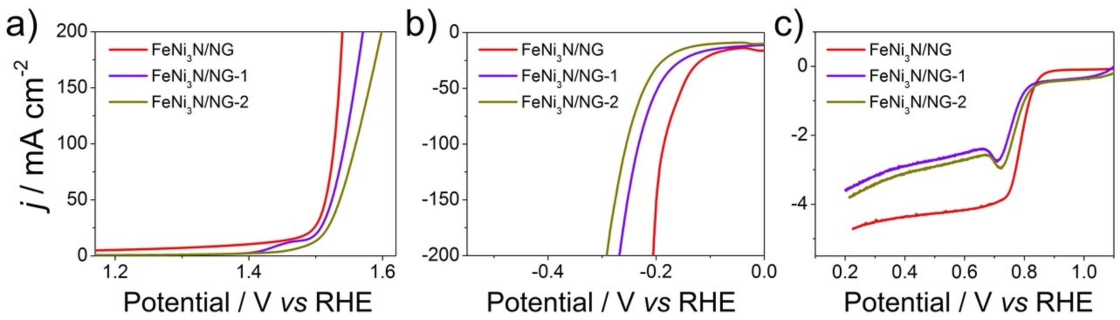

Fig. S18. (a) The polarization curves of $FeNi_3N$/NG, $FeNi_3N$/NG-1, and $FeNi_3N$/NG-2 toward OER in 1.0 M KOH. (a) The polarization curves of $FeNi_3N$/NG, $FeNi_3N$/NG-1, and $FeNi_3N$/NG-2 toward HER in 1.0 M KOH. (a) The polarization curves of $FeNi_3N$/NG, $FeNi_3N$/NG-1, and $FeNi_3N$/NG-2 toward ORR in 0.1 M KOH.

Table S1. Comparison of electrocatalytic activity of the FeNi$_3$N/NG with recently reported highly active ORR/OER bifunctional oxygen electrode materials.

Catalysts	half-wave potential ($E_{1/2}$ / V)	OER Overpotential at 10 mA cm^{-2} (V vs RHE)	ΔE / V	Electrolyte concentration (pH)	Ref.
FeNi$_3$N/NG	0.79	0.41	0.85	13	This work
NiCo$_2$S$_4$@graphene	0.76	0.47	0.94	13	S4
NCNF-1000	0.82	0.61	1.02	13	S5
N, S-CN	0.77	0.45	0.88	13	S6
N-doped graphene/CNT	0.63	0.4	1.0	13	S7
Mn$_x$O$_y$/N-doped carbon	0.81	0.45	0.87	13	S8
PCN-CFP	0.67	0.4	0.96	13	S9
Fe@N-C	0.83	0.48	0.88	13	S10
Co$_3$O$_4$/Co$_2$MnO$_4$ nanocomposite	0.68	0.54	1.09	13	S11
NiO/CoN PINWs	0.68	0.3	0.85	13	S12

Table S2. Comparison of the primary Zn-air batteries performance of FeNi$_3$N/NG with various catalysts in the recent literature.

Catalysts	Capacity (mAhg^{-1} at 10 mAcm^{-2})	Power density (Mw cm^{-2})	Ref.
FeNi$_3$N/NG	785.2	115.3	This work
NCNT/Co$_x$Mn$_{1-x}$O	581 (7mA/cm^2)	—	S13
N-doped carbon nanotubes	—	69.5	S14
NCNF-1000	626	185	S5
NiFe@NC$_X$	583.7	~85	S15
Cu-Pt nanocage	560	—	S16
Fe@C-NG/NCNTs	682.6	101.2	S17
C-MOF-C2-900	741	105	S18

Table S3. The performance comparison of rechargeable solid-state zinc-air batteries with $FeNi_3N$/NG electrodes with recently reported catalytic electrodes.

Catalysts	Open circuit voltage (V)	Rechargeability (10 mA cm^{-2})	Ref.
$FeNi_3N$/NG	1.463	600 s/cycle for 60 cycles	This work
NCNF-1000	1.256	600 s/cycle for 36 cycles (2 mA cm^{-2})	S5
$CuCo_2O_4$/N-CNTs	1.24	1200 s/cycle for 27 cycles	S19
NC-Co_3O_4-90	1.44	1200 s/cycle for 60 cycles (1 mA cm^{-2})	S20
Co-N,B-CSs	1.345	—	S21
FeCo nanoparticles enveloped by N-doped graphitic CNTs	1.25	600 s/cycle for 72 cycles (100 mA cm^{-2})	S22
Meso-CoNC@GF	1.4	600 s/cycle for 70 cycles	S23

Table S4. Comparison of OER activity of the $FeNi_3N$/NG with recently reported catalyst.

Catalysts	Overpotential at 20 mA cm^{-2} (mV)	Overpotentialat 100 mA cm^{-2} (mV)	Tafel slope (mv dec^{-1})	Electrolyte concentration (pH)	Ref.
$FeNi_3N$/NG	258	298	45.3	14	This work
CoPh/NG	300	343	54	14	S24
NiFeB	η_{10}=251	—	43	14	S25
$NiCo_2S_4$/CC	280	340	89	14	S26
TiN@Ni_3N nanowire arrays	η_{10}=350	>400	93.7	14	S27
NiCoP-NWAs/NF	270	370	116	14	S28
Zn-Co-S/TM	330	>370	79	14	S29
NiMoN-550	321	390	94	14	S30
$NiCo_2S_4$ NW/GDF	308	338	47	14	S31

Table S5. Comparison of HER activity of the $FeNi_3N/NG$ with recently reported catalyst.

Catalysts	Overpotential at 20 mA cm^{-2} (mV)	Overpotentialat 100 mA cm^{-2} (mV)	Tafel slope (mv dec^{-1})	Electrolyte concentration (pH)	Ref.
$FeNi_3N/NG$	98	186	83.1	14	This work
V/NF	203	~220	82	14	S32
NiS/Ni foam	158	>200	83	14	S33
Zn-Co-S/TM	238	>300	164	14	S29
Co_3Se_4/CF	225	262	72	14	S34
$FeNi_3N/NF$	η_{10}=75	>200	98	14	S35
NiMoN-550	159	265	79	14	S30
$NiCo_2S_4$ NW/GDF	170	253	92	14	S31

Table S6. Comparison of the electrochemical performance of $FeNi_3N/NG|FeNi_3N/NG$ as bifunctional catalysts for overall water splitting in 1.0 M KOH with recently published results.

Catalysts	voltage at 20 mA cm^{-2} (V)	Electrolyte concentration (pH)	Ref.
$FeNi_3N/NG$	1.585	14	This work
NiCoP NWAs/NF	1.64	14	S28
CoOx-CoSe/NF	1.66	14	S36
NiMoN-550	η_{10}=1.596	14	S30
V/NF	1.8	14	S32
Co_3Se_4/CF	1.63	14	S34
TiN@Ni_3N nanowire arrays	1.69	14	S27
FeNi/NPC	η_{10}=1.63	14	S37

Table S7. Nitrogen contents in the Ni-N/NG and $FeNi_3N/NG$.

Catalyst	Metal-N (at%)	Pyridinic-N (at%)	Pyrrolic-N (at%)	Graphitic-N (at%)	Oxide-N (at%)	Total (at%)
Ni-N/NG	0.64	1.66	1.96	0.13	0.44	4.83
$FeNi_3N/NG$	0.21	2.33	0.35	0.95	0.19	4.03

REFERENCES

1. Clark, S. J.; Segall, M. D.; Pickard, C. J.; Hasnip, P. J.; Probert, M. J.; Refson, K.; Payne, M. C. First Principles Methods Using CASTEP. *Zeitschrift fuer Kristallographie*. **2005**, *220*, 567-570.
2. Perdew, J. P. in Electronic Structure of Solids ’91, Ed. Ziesche,P. and Eschrig,H. (Akademie-Verlag, Berlin, **1991**) *11*.
3. Perdew, J. P.; Wang, Y. Accurate and Simple Analytic Representation of the Electron-gas Correlation Energy. *Phys. Rev. B.* **1992**, *45*, 13244-13249.
4. Liu, Q.; Jin, J. T.; Zhang, J. Y. $NiCo_2S_4$@graphene as a Bifunctional Electrocatalyst for Oxygen Reduction and Evolution Reactions. *ACS Appl. Mater. Interfaces* **2013**, *5*, 5002-5008.
5. Liu, Q.; Wang, Y. B.; Dai, L. M.; Yao, J. N. Scalable Fabrication of Nanoporous Carbon Fiber Films as Bifunctional Catalytic Electrodes for Flexible Zn-Air Batteries. *Adv. Mater.* **2016**,*28*, 3000-3006.
6. Qu, K. G.; Zheng, Y.; Dai, S.; Qiao, S. Z. Graphene Oxide-polydopamine Derived N,S-codoped Carbon Nanosheets as Superior Bifunctional Electrocatalysts for Oxygen Reduction and Evolution. *Nano Energy* **2016**, *19*, 373-381.
7. Tian, G.-L.; Zhao, M.-Q.; Yu, D. S.; Kong, X.-Y.; Huang, J.-Q.; Zhang, Q.; Wei, F. Nitrogen-Doped Graphene/Carbon Nanotube Hybrids: In Situ Formation on Bifunctional Catalysts and Their Superior Electrocatalytic Activity for Oxygen Evolution/Reduction Reaction. *Small* **2014**,*10*, 2251-2259.
8. Masa, J.; Xia, W.; Sinev, I.; Zhao, A. Q.; Sun, Z. Y.; Grützke, S.; Weide, P.;

Muhler, M.; Schuhmann, W. Mn_xO_y/NC and Co_xO_y/NC Nanoparticles Embedded in a Nitrogen-Doped Carbon Matrix for High-Performance Bifunctional Oxygen Electrodes. *Angew. Chem. Int. Ed.* **2014**, *53*, 8508-8512.

9. Ma, T. Y.; Ran, J. R.; Dai, S.; Jaroniec, M.; Qiao, S. Z. Phosphorus-doped Graphitic Carbon Nitrides Grown In Situ on Carbon-fiber Paper: Flexible and Reversible Oxygen Electrodes. *Angew. Chem. Int. Ed.* **2015**, *54*, 4646-4650.
10. Wang, J.; Wu, H. H.; Gao, D. F.; Miao, S.; Wang, G. X.; Bao, X. H.High-density Iron Nanoparticles Encapsulated within Nitrogen-doped Carbon Nanoshell as Efficient Oxygen Electrocatalyst for Zinc-Air Battery. *Nano Energy* **2015**, *13*, 387-396.
11. Wang, D. D.; Chen, X.; Evans, D. G.; Yang, W. S. Well-dispersed Co_3O_4/Co_2MnO_4Nanocomposites as a Synergistic Bifunctional Catalyst for Oxygen Reduction and Oxygen Evolution Reactions. *Nanoscale* **2013**, *5*, 5312-5315.
12. Yin, J.; Li, Y. X.; Lv, F.; Fan, Q. H.; Zhao,Y.-Q.; Zhang, Q. L.; Wang, W.; Cheng, F. Y.; Xi, P. X.; Guo, S. J. NiO/CoN Porous Nanowires as EfficientBifunctional Catalysts for Zn-Air Batteries. *ACS Nano* **2017**, *11*, 2275-2283.
13. Liu, X.; Park, M.; Kim, M. G.; Gupta, S.; Wang, X. J.; Wu, G.; Cho, J. High-performance Non-spinel Cobalt-manganese Mixed Oxide-based Bifunctional Electrocatalysts for Rechargeable Zinc-Air Batteries. *Nano Energy* **2016**, *20*, 315-325.

14. Zhu, S. M.; Chen, Z.; Li, B.; Higgins, D.; Wang, H. J.; Li, H.; Chen, Z. W. Nitrogen-doped Carbon Nanotubes as Air Cathode Catalysts in Zinc-Air Battery. *Electrochimica Acta* **2011**, *56*, 5080-5084.

15. Zhu, J. B.; Xiao, M. L.; Zhang, Y. L.; Jin, Z.; Peng, Z. Q.; Liu, C. P.; Chen, S. L.; Ge, J. J.; Xing, W. Metal-Organic Framework-Induced Synthesis of Ultrasmall Encased NiFe Nanoparticles Coupling with Graphene as an Efficient Oxygen Electrode for a Rechargeable Zn-Air Battery. *ACS Catal.* **2016**, *6*, 6335-6342.

16. Dhavale, V. M.; Kurungot, S. Cu-Pt Nanocage with 3-D Electrocatalytic Surface as an Efficient Oxygen Reduction Electrocatalyst for a Primary Zn-Air Battery. *ACS Catal.* **2015**, *5*, 1445-1452.

17. Wang, Q. C.; Lei, Y. P.; Chen, Z. Y.; Wu, N.; Wang, Y. B.; Wang, B.; Wang, Y. D. Fe/Fe_3C@C Nanoparticles Encapsulated in N-doped Graphene-CNTs Framework as an Efficient Bifunctional Oxygen Electrocatalyst for Robust Rechargeable Zn-Air Batteries. *J. Mater. Chem. A* **2018**, *6*, 516-526.

18. Zhang, M. D.; Dai, Q. B.; Zheng, H. G.; Chen, M. D.; Dai, L. M. Novel MOF-Derived Co@N-C Bifunctional Catalysts for Highly Efficient Zn-Air Batteries and Water Splitting. *Adv. Mater.* **2018**, *30*, 1705431.

19. Cheng, H.; Li, M.-L.; Su, C.-Y.; Li, N.; Liu, Z.-Q. Cu-Co Bimetallic Oxide Quantum Dot Decorated Nitrogen-Doped Carbon Nanotubes: A High-Efficiency Bifunctional Oxygen Electrode for Zn-Air Batteries. *Adv. Funct. Mater.* **2017**, *27*, 1701833.

20. Guan, C.; Sumboja, A.; Wu, H. J.; Ren, W. N.; Liu, X. M.; Zhang, H.; Liu, Z. L.;

Cheng, C. W.; Pennycook, S. J.; Wang, J. Hollow Co_3O_4 Nanosphere Embedded in Carbon Arrays for Stable and Flexible Solid-State Zinc-Air Batteries. *Adv. Mater.* **2017**, *29*, 1704117.

21. Guo, Y. Y.; Yuan, P. F.; Zhang, J. N.; Hu, Y. F.; Amiinu, I. S.; Wang, X.; Zhou, J. G.; Xia, H. C.; Song, Z. B.; Xu, Q.; Mu, S. C. Carbon Nanosheets Containing Discrete Co-N_x-B_y-C Active Sites for Efficient Oxygen Electrocatalysis and Rechargeable Zn-Air Batteries. *ACS Nano* **2018**, *12*, 1894-1901.
22. Su, C.-Y.; Cheng, H.; Li, W.; Liu, Z.-Q.; Li, N.; Hou, Z. F.; Bai, F.-Q.; Zhang, H.-X.; Ma, T.-Y. Atomic Modulation of FeCo-Nitrogen-Carbon Bifunctional Oxygen Electrodes for Rechargeable and Flexible All-Solid-State Zinc-Air Battery. *Adv. Energy Mater.* **2017**, *7*, 1602420.
23. Liu, S. S.; Wang, M. F.; Sun, X. Y.; Xu, N.; Liu, J.; Wang, Y. Z.; Qian, T.; Yan, C. L. Facilitated Oxygen Chemisorption in Heteroatom-Doped Carbon for Improved Oxygen Reaction Activity in All-Solid-State Zinc-Air Batteries. *Adv. Mater.* **2018**, *30*, 1704898.
24. Yu, X. B.; Zhang, S.; Li, C. Y.; Zhu, C. L.; Chen, Y. J.; Gao, P.; Qi, L. H.; Zhang, X. T. Hollow CoP Nanopaticle/N-doped Graphene Hybrids as Highly Active and Stable Bifunctional Catalysts for Full Water Splitting. *Nanoscale* **2016**, *8*, 10902-10907.
25. Liu, G.; He, D. Y.; Yao, R.; Zhao, Y.; Li, J. P. Amorphous NiFeB Nanoparticles Realizing Highly Active and Stable Oxygen Evolving Reaction for Water Splitting. *Nano Research* **2018**, *11*, 1664-1675.

26. Liu, D. N.; Lu, Q.; Luo, Y. L.; Sun, X. P.; Asiri, A. M. $NiCo_2S_4$Nanowires Array as an Efficient Bifunctional Electrocatalyst for Full Water Splitting with Superior Activity. *Nanoscale* **2015**, *7*, 15122-15126.

27. Zhang, Q. T.; Wang, Y. H.; Wang, Y. C.; Al-Enizi, A. M.; Elzatahry, A. A.; Zheng, G. F. Myriophyllum-like Hierarchical TiN@Ni_3N Nanowire Arrays for Bifunctional Water Splitting Catalysts. *J. Mater. Chem. A* **2016**, *4*, 5713-5718.

28. Li, J. Z.; Wei, G. D.; Zhu, Y. K.; Xi, Y. L.; Pan, X. X.; Ji, Y.; Zatovsky, I. V.; Han, W. Hierarchical NiCoP Nanocone Arrays Supported on Ni foam as an Efficient and Stable Bifunctional Electrocatalyst for Overall Water Splitting. *J. Mater. Chem. A* **2017**, *5*, 14828-14837.

29. Liang, Y. H.; Liu, Q.; Luo, Y. L.; Sun, X. P.; He, Y. Q.; Asiri, A. M. $Zn_{0.76}Co_{0.24}S/CoS_2$Nanowires Array for Efficient Electrochemical Splitting of Water. *Electrochimica Acta* **2016**, *190*, 360-364.

30. Yin, Z. X.; Sun, Y.; Zhu, C. L.; Li, C. Y.; Zhang, X. T.; Chen, Y. J. Bimetallic Ni-Mo Nitride Nanotubes as Highly Active and Stable Bifunctional Electrocatalysts for Full Water Splitting. *J. Mater. Chem. A* **2017**, *5*, 13648-13658.

31. Xue, Y. R.; Zuo, Z. C.; Li, Y. J.; Liu, H. B.; Li, Y. L. Graphdiyne-Supported $NiCo_2S_4$ Nanowires: A Highly Active and Stable 3D Bifunctional Electrode Material. *Small* **2017**, *13*, 1700936.

32. Yu, Y.; Li, P.; Wang, X. F.; Gao, W. Y.; Shen, Z. X.; Zhu, Y. N.; Yang, S. L.; Song, W. G.; Ding, K. J. Vanadium Nanobelts Coated Nickel Foam 3D Bifunctional Electrode with Excellent Catalytic Activity and Stability for Water

Electrolysis. *Nanoscale* **2016**, *8*, 10731-10738.

33. Zhu, W. X.; Yue, X. Y.; Zhang, W. T.; Yu, S. X.; Zhang, Y. H.; Wang, J.; Wang, J. L. Nickel Sulfide Microsphere Film on Ni foam as an Efficient Bifunctional Electrocatalyst for Overall Water Splitting. *Chem.Commun.* **2016**, *52*, 1486-1489.
34. Li, W.; Gao, X. F.; Xiong, D. H.; Wei, F.; Song, W. G.; Xu, J. Y.; Liu, L. F. Hydrothermal Synthesis of Monolithic Co_3Se_4 Nanowire Electrodes for Oxygen Evolution and Overall Water Splitting with High Efficiency and Extraordinary Catalytic Stability. *Adv. Energy Mater.* **2017**, *7*, 1602579.
35. Zhang, B.; Xiao, C. H.; Xie, S. M.; Liang, J.; Chen, X.; Tang, Y. H. Iron-Nickel Nitride Nanostructures in Situ Grown on Surface-Redox-Etching Nickel Foam: Efficient and Ultrasustainable Electrocatalysts for Overall Water Splitting. *Chem. Mater.* **2016**, *28*, 6934-6941.
36. Xu, X. J.; Du, P. Y.; Chen, Z. K.; Huang, M. H. An Electrodeposited Cobalt-selenide-based Film as an Efficient Bifunctional Electrocatalyst for Full Water Splitting. *J. Mater. Chem. A* **2016**, *4*, 10933-10939.
37. Zhong, H.-X.; Wang, J.; Zhang, Q.; Meng, F. L.; Bao, D.; Liu, T.; Yang, X.-Y.; Chang, Z.-W.; Yan, J.-M.; Zhang, X.-B. In Situ Coupling FeM (M = Ni, Co) with Nitrogen-Doped Porous Carbon toward Highly Efficient Trifunctional Electrocatalyst for Overall Water Splitting and Rechargeable Zn-Air Battery. *Adv. Sustainable Syst.* **2017**, *1*, 1700020.